# Numerical Boundary Condition Procedures for Euler Solvers

David L. Marcum* and Joe D. Hoffman†
*Purdue University, West Lafayette, Indiana*

**A numerical boundary condition procedure for Euler solvers is presented. The procedure is based on a variation of the method of characteristics due to Kentzer. A second-order-accurate numerical algorithm using this procedure and the MacCormack explicit finite-difference method is presented. Results are presented for several two-dimensional and three-dimensional inviscid nozzle flowfields. Solutions obtained by the present method agree well with solutions obtained by method of characteristics algorithms and experimental data.**

## Introduction

In recent years, the importance of careful implementation of the boundary conditions in computational fluid dynamics has become more apparent.[1] As demonstrated by Abbett[2] for steady two-dimensional supersonic flow, the method of characteristics is the superior procedure for this purpose. The objectives of the present investigation were to investigate numerical boundary condition procedures for unsteady inviscid flow (i.e., Euler) solvers and to develop an accurate, efficient, and compatible boundary condition procedure based on the method of characteristics for use with finite-difference methods.

There are three primary advantages of the method of characteristics:

1) It identifies the physical paths of propagation of information through a flowfield, which are the pathline and the wave surfaces.

2) It identifies which characteristic compatibility equations are applicable at a boundary point where the applicable equations include both the governing differential equations of motion and the boundary conditions. Thus, the applicable equations overspecify the problem. The method of characteristics can be used to determine an equivalent set of characteristic compatibility equations, including the boundary conditions, without overspecifying the problem.

3) It can be used as a numerical scheme. In the numerical method of characteristics, the computational coordinates are the paths of propagation of information, which results in an extremely accurate modeling of the flowfield.

The numerical method of characteristics is, unfortunately, a complicated numerical procedure that requires much more developmental effort and greater computational time than most finite-difference or finite-volume methods. A variation of the method of characteristics due to Kentzer[3] can be employed to implement boundary conditions with almost any finite-difference scheme. The Kentzer method retains the first two aforementioned advantages of the method of characteristics, is straightforward to implement, and is computationally efficient. Hoffman and Brown[4] have successfully employed the Kentzer method at solid boundary points to solve unsteady three-dimensional transonic flowfields in axisymmetric propulsive nozzles with rotation. Chakravarthy[5] has employed the method of characteristics in a manner similar to Kentzer to develop implicit boundary conditions for unsteady two-dimensional inviscid flow. An extension of the Kentzer method is used in the present investigation to implement all of the boundary conditions required to solve nozzle flowfields.

Presented as Paper 86-0107 at the AIAA 24th Aerospace Sciences Meeting, Reno, NV, Jan. 6-9, 1986; received Jan. 27, 1986; revision received Dec. 10, 1986. 

*Research Associate, Mechanical Engineering, Thermal Sciences and Propulsion Center. Presently Senior Specialist Engineer, Boeing Commercial Airplane Company, Seattle, WA. Member AIAA.

†Professor of Mechanical Engineering, Thermal Sciences and Propulsion Center. Associate Fellow AIAA.

## Gas Dynamic Model

The gas dynamic model is based on the following assumptions: 1) unsteady three-dimensional flow, 2) inviscid nonconducting fluid with no body forces, and 3) a simple system in thermodynamic equilibrium. The governing equations consist of the continuity equation, the vector momentum equation, the energy equation, and the thermal and caloric equations of state.

The governing equations can be expressed in either primitive or conservative variables. In the present investigation, the boundary conditions are implemented using the method of characteristics. The characteristic compatibility equations are expressed in primitive variables. Consequently, the governing equations in primitive variables are employed. They are

$$\rho_t = -\bar{V}\cdot\nabla\rho - \rho\nabla\cdot\bar{V} = C \tag{1}$$

$$\bar{V}_t = -\bar{V}\cdot\nabla\bar{V} - \nabla P/\rho = \bar{M} \tag{2}$$

$$P_t - a^2\rho_t = -\bar{V}\cdot\nabla P + a^2\bar{V}\cdot\nabla\rho = E \tag{3}$$

where $t$ denotes time, $\rho$ the density, $\bar{V}$ the velocity vector, $P$ the pressure, $a$ the speed of sound, and $C$, $\bar{M}$, and $E$ denote the space derivatives appearing in the continuity, momentum, and energy equations, respectively. The density derivatives in the energy equation, Eq. (3), can be eliminated by combining Eqs. (1) and (3) to obtain

$$P_t = E + a^2C \tag{4}$$

The speed of sound is specified by the functional relationship $a = a(P,\rho)$.

## Characteristic Equations

The governing equations for the present investigation, Eqs. (1-3), comprise a set of hyperbolic quasilinear partial-differential equations of the first order. The method of characteristics can be employed to form linear combinations of such a set of equations to obtain an equivalent set of characteristic compatibility equations that are valid only in

corresponding characteristic surfaces. A characteristic surface is a surface in the solution space on which the governing partial-differential equations may be combined linearly to form a characteristic compatibility equation. A characteristic compatiblity equation is an interior operator that has one less independent variable, contains derivatives only in the corresponding characteristic surface, and is valid only in the corresponding characteristic surface. Rusanov,[6] Hoffman,[7] and Zucrow and Hoffman[8] present detailed derivations of the characteristic compatibility equations for an unsteady flow. A summary of those results is presented in the following discussion.

For unsteady three-dimensional flow there are four independent variables. The characteristic surfaces are hypersurfaces in four-dimensional space. There are two families of characteristic hypersurfaces: the stream hypersurfaces and the wave hypersurfaces. There are two types of characteristic hypercurves corresponding to the two families of characteristic hypersurfaces: the pathline and wavelines. The pathline is the envelope of all stream hypersurfaces at a point. The envelope of all wave hypersurfaces at a point is the Mach hyperconoid. A waveline is the hyperline of contact between a wave hypersurface and the Mach hyperconoid.

A characteristic compatibility equation contains directional derivatives only along a characteristic hypercurve or in the corresponding characteristic hypersurface. The directional derivative along a characteristic hypercurve is given by

$$\left.\frac{\mathrm{d}(\ )}{\mathrm{d}t}\right|_{\bar{W}} = (\ )_t + \bar{W}\cdot\nabla(\ ) \tag{5}$$

where $\bar{W}$ is the relative velocity along the hypercurve. There are two characteristic compatibility equations corresponding to the two characteristic hypercurves: the pathline equation and the waveline equation.

The pathline equation must contain directional derivatives only along the pathline or in a stream hypersurface. The relative velocity along a pathline is the fluid velocity. Thus, the directional derivative along the pathline is given by

$$\frac{\mathrm{D}(\ )}{\mathrm{D}t} = (\ )_t + \bar{V}\cdot\nabla(\ ) \tag{6}$$

which is the conventional substantial derivative. The energy equation, Eq. (3), is a characteristic compatibility equation, as it contains directional derivatives only along the pathline. Substituting Eq. (6) into Eq. (3) yields the pathline equation

$$\frac{\mathrm{D}P}{\mathrm{D}t} - a^2\frac{\mathrm{D}\rho}{\mathrm{D}t} = 0 \tag{7}$$

The waveline equation must contain directional derivatives only along a waveline or in the corresponding wave hypersurface. The relative velocity along a waveline is

$$\bar{W} = \bar{V} - a\bar{n}_i \tag{8}$$

where $\bar{n}_i$ is the unit vector normal to the corresponding wave hypersurface. Thus, the directional derivative along a waveline is given by

$$\frac{\mathfrak{D}(\ )}{\mathfrak{D}t} = (\ )_t + (\bar{V} - a\bar{n}_i)\cdot\nabla(\ ) \tag{9}$$

The governing equations, Eqs. (1-3), can be combined as follows to obtain the waveline equation:

$$a^2[\text{Eq.}(1)] - \rho a\bar{n}_i\cdot[\text{Eq.}(2)] + [\text{Eq.}(3)] = 0 \tag{10}$$

Substituting Eqs. (1-3) and (9) into Eq. (10) yields the waveline equation

$$\frac{\mathfrak{D}P}{\mathfrak{D}t} - \rho a\bar{n}_i\cdot\frac{\mathfrak{D}\bar{V}}{\mathfrak{D}t} + \rho a^2[\mathrm{d}_{\bar{\ell}}(\bar{V}\cdot\bar{\ell}) + \mathrm{d}_{\bar{m}}(\bar{V}\cdot\bar{m})] = 0 \tag{11}$$

where $\bar{\ell}$ and $\bar{m}$ are unit vectors tangent to the wave hypersurface and orthogonal to $\bar{n}_i$. The waveline equation contains directional derivatives along the waveline and in the wave hypersurface corresponding to wave hypersurface unit normal $\bar{n}_i$.

The pathline equation, Eq. (7), is valid on the pathline. The waveline equation, Eq. (11), is valid in the wave hypersurface corresponding to wave hypersurface unit normal vector $\bar{n}_i$. There are an infinite number of wave hypersurface unit normal vectors $\bar{n}_i$ corresponding to the infinite number of wave hypersurfaces at a point. Since there are only five independent governing equations for unsteady three-dimensional flow [i.e., Eqs. (1-3)], only five characteristic compatibility equations can be included in an independent set of equations. The pathline equation must be included as it is the only characteristic compatibility equation that contains a derivative of density. Consequently, four and only four waveline characteristic compatibility equations are independent for unsteady three-dimensional flow. Rusanov[6] has shown that the pathline equation [Eq. (7)], applied along the pathline, and the waveline equation [Eq. (11)], applied in any four independent wave hypersurfaces, comprise one set of independent characteristic compatibility equations equivalent to the original set of governing equations, Eqs. (1-3).

The wave hypersurface unit normal vectors $\bar{n}_i$ $(i=1,2,3,4)$ corresponding to four independent wave hypersurfaces can be expressed in terms of a local set of orthogonal unit vectors aligned with a boundary as follows:

$$\bar{n}_i = n_{i,b}\bar{b} + n_{i,t}\bar{t} + n_{i,s}\bar{s} \tag{12}$$

where $\bar{b}$ is the unit vector normal to the boundary and $\bar{t}$ and $\bar{s}$ are unit vectors tangent to the boundary and orthogonal to $\bar{b}$.

In the Kentzer method,[3] the directional derivatives appearing in the characteristic compatibility equations are expressed in partial derivative form. The resulting equations are used only at boundary points and are solved by the same numerical scheme that is employed at interior points. Expressing the directional derivatives in the pathline equation and the waveline equation in partial derivative form and rearranging yields

$$P_t - a^2\rho_t = E \tag{13}$$

$$P_t - \rho a\bar{n}_i\cdot\bar{V}_t = E + a^2C - \rho a\bar{n}_i\cdot\bar{M} \tag{14}$$

At boundary points, the governing equations, Eqs. (1-3), are replaced with the pathline equation, Eq. (13), and the waveline equation, Eq. (14), applied in four independent wave hypersurfaces. At interior points the same set of characteristic compatibility equations could be used, but they reduce to the original set of governing equations, Eqs. (1-3). It is only when one or more boundary conditions replace one or more characteristic compatibility equations that the resulting set of equations differs from the original set of governing equations.

In the present investigation, the Kentzer method[3] is extended by forming linear combinations of the applicable characteristic compatibility equations and boundary conditions at boundary points. These linear combinations result in a new set of equations that applies at boundary points. In most cases, this new set of equations is similar to the original set of equations that applies at interior points.

## Boundary Point Equations

A variety of flowfield unit processes are employed in the computation of a flowfield. There are four basic types of flowfield unit processes considered in the present investigation: interior points, free-slip solid boundary points, exit boundary points, and inlet boundary points. Brief descriptions of the applicable equations at the boundary points are presented in the following discussion. Detailed descriptions and the derivations of the applicable equations for these and other flowfield unit processes are presented in Ref. 9.

The boundary point equations developed in the following discussion are obtained by combining the pathline equation, Eq. (13), an appropriate set of waveline equations, Eq. (14), and the appropriate boundary conditions. The number of applicable waveline equations depends on the type of boundary point. The exact orientation of the wave hypersurface unit normal vectors $\bar{n}_i$ $(i=1,2,3,4)$ is not important. All that is important is whether each particular unit normal vector $\bar{n}_i$ $(i=1,2,3,4)$ points inside or outside of the computational flowfield.

The boundary point equations developed in the following discussion are reduced from the applicable characteristic compatibility equations and boundary conditions to forms similar to the equations that apply at an interior point. This results in accurate and efficient boundary point unit processes that are extremely compatible with the interior point unit process.

### Solid Boundary Point Equations

The boundary condition applicable at a free-slip solid boundary point is that the velocity normal to the boundary is zero. Thus,

$$\bar{b}\cdot\bar{V}=0 \tag{15}$$

where $\bar{b}$ is the outward-pointing unit vector normal to the solid boundary. Differentiating Eq. (15) with respect to time yields

$$\bar{b}\cdot\bar{V}_t=0 \tag{16}$$

The governing equations, Eqs. (1-3), are replaced with the equivalent characteristic compatibility equations, Eqs. (13) and (14), at a free-slip solid boundary point. The waveline equation is applied in four wave hypersurfaces corresponding to the wave hypersurface unit normal vectors $\bar{n}_i(i=1,2,3,4)$ given by Eq. (12). The wave hypersurface unit normal vectors $\bar{n}_i(i=1,2,3)$ are chosen such that they are in directions pointing inside the flowfield. The wave hypersurface unit normal vector $\bar{n}_4$ is chosen such that it is in a direction pointing outside of the flowfield. Thus, the wave hypersurface corresponding to the wave hypersurface unit normal vector $\bar{n}_4$ is outside of the flowfield, and the waveline equation corresponding to that wave hypersurface unit normal vector is discarded and replaced with the boundary condition, Eq. (16). This situation is illustrated for unsteady two-dimensional flow in Fig. 1.

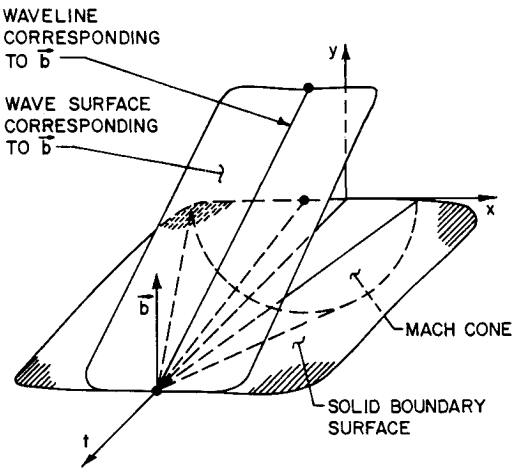


**Fig. 1 Solid boundary point unit process.**

The applicable equations at a free-slip solid boundary point are the pathline equation, Eq. (13), the waveline equation, Eq. (14), applied in three wave hypersurfaces corresponding to wave hypersurface unit normal vectors $\bar{n}_i$ $(i=1,2,3)$, and the boundary condition, Eq. (16). The three waveline equations can be combined to yield

$$\bar{t}\cdot\bar{V}_t=\bar{t}\cdot\bar{M}+c_1B \tag{17}$$

$$\bar{s}\cdot\bar{V}_t=\bar{s}\cdot\bar{M}+c_2B \tag{18}$$

$$P_t=E+a^2C+c_3\rho aB \tag{19}$$

where

$$B=\bar{b}\cdot(\bar{V}_t-\bar{M}) \tag{20}$$

and $c_1$, $c_2$, and $c_3$ are constants determined by the choice of wave hypersurface unit normal vectors $\bar{n}_i$ $(i=1,2,3)$. The component of the vector momentum equation normal to the boundary, Eq. (20), is equal to zero. Thus, linear combinations of the applicable equations, Eqs. (13), (16), and (17-19), can be formed which are similar to the governing equations at an interior point. These linear combinations result in a new set of equations applicable at a solid boundary point. They are

$$\rho_t=C \tag{21}$$

$$\bar{V}_t=\bar{t}(\bar{t}\cdot\bar{M})+\bar{s}(\bar{s}\cdot\bar{M}) \tag{22}$$

$$P_t=E+a^2C \tag{23}$$

where $\bar{t}$ and $\bar{s}$ are any two unit vectors tangent to the solid boundary and orthogonal to $\bar{b}$. Equation (21) is the continuity equation, Eq. (22) is the vector momentum equation projected onto the boundary surface, and Eq. (23) is a linear combination of the energy equation and the continuity equation. Consequently, the applicable equations at a solid boundary point differ from those at an interior point only in that the projection of the vector momentum equation onto the boundary surface is used instead of the general vector momentum equation.

### Exit Boundary Point Equations

Two types of exit boundary points were considered in the present investigation: subsonic exit boundary points and supersonic exit boundary points. At a subsonic exit boundary point, the velocity normal to the exit boundary is less than the speed of sound. The boundary condition applicable at a subsonic exit boundary point is that the static pressure is known. Thus,

$$P=P_{\text{exit}} \tag{24}$$

The governing equations, Eqs. (1-3), are replaced with the equivalent characteristic compatibility equations, Eqs. (13) and (14), at a subsonic exit boundary point. The waveline equation, Eq. (14), is applied in four wave hypersurfaces corresponding to the wave hypersurface unit normal vectors $\bar{n}_i$ $(i=1,2,3,4)$ given by Eq. (12). The wave hypersurface unit normal vectors $\bar{n}_i$ $(i=1,2,3)$ are chosen such that they are in directions pointing inside the computational flowfield. The wave hypersurface unit normal vector $\bar{n}_4$ is chosen such that it is in a direction pointing outside of the computational flowfield. Thus, the wave hypersurface corresponding to wave hypersurface unit normal vector $\bar{n}_4$ is outside of the

computational flowfield, and the waveline equation corresponding to that wave hypersurface is discarded and replaced with the boundary condition, Eq. (24). This situation is illustrated for unsteady two-dimensional flow in Fig. 2.

The applicable equations at a subsonic exit boundary point are the pathline equation, Eq. (13), the waveline equation, Eq. (14), applied in three wave hypersurfaces corresponding to wave hypersurface unit normal vectors $\bar{n}_i$ $(i=1,2,3)$, and the boundary condition, Eq. (24). The three waveline equations can be combined to yield

$$\bar{V}_t = \bar{M} + \bar{c}\frac{P_t - E - a^2 C}{\rho a} \tag{25}$$

where $\bar{c}$ is a vector determined by the choice of wave hypersurface unit normal vectors $\bar{n}_i$ $(i=1,2,3)$. The combined energy and continuity equation, Eq. (4), which appears in Eq. (25), is equal to zero. Thus, linear combinations of the applicable equations, Eqs. (13), (24), and (25), can be formed which are similar to the governing equations at an interior point. These linear combinations result in a new set of equations applicable at a subsonic exit boundary point. They are

$$\rho_t = (P_{\text{exit},t} - E)/a^2 \tag{26}$$

$$\bar{V}_t = \bar{M} \tag{27}$$

$$P = P_{\text{exit}} \tag{28}$$

Equation (26) is the energy equation and Eq. (27) is the vector momentum equation. Consequently, the applicable equations at a subsonic exit boundary point differ from those at an interior point in that the energy equation is used instead of the combined energy and continuity equation, the continuity equation is not used, and the static pressure $P_{\text{exit}}$ is specified. The partial derivative with respect to time of the static pressure appearing in Eq. (26) must be specified.

At a supersonic exit boundary point, the velocity normal to the exit boundary is greater than or equal to the speed of sound. The governing equations, Eqs. (1-3), are replaced with the equivalent characteristic compatibility equations, Eqs. (13) and (14). The waveline equation, Eq. (14), is applied in four wave hypersurfaces corresponding to the wave hypersurface unit normal vectors $\bar{n}_i$ $(i=1,2,3,4)$ given by Eq. (12). The four wave hypersurfaces and the pathline are all inside the computational flowfield. Thus no boundary condition is required. Consequently, the governing equations are identical to those used in the interior point unit process, Eqs. (1), (2), and (4).

#### Inlet Boundary Point Equations

Two types of inlet boundary points were considered in the present investigation: subsonic inlet boundary points and supersonic inlet boundary points. At a subsonic inlet boundary point, the velocity normal to the inlet boundary is less than the speed of sound. The boundary conditions applicable at a subsonic inlet boundary point are that the stagnation temperature $T_0$, the stagnation pressure $P_0$, and the flow angles are known. The stagnation temperature and the stagnation pressure are related to the flow properties by the functional relationships

$$T_0 = T_0(P, \rho, V) \tag{29}$$

$$P_0 = P_0(P, \rho, V) \tag{30}$$

where $V$ is the velocity magnitude. The velocity vector can be related to the velocity component normal to the inlet boundary by

$$\bar{V} = \bar{\delta}(\bar{b} \cdot \bar{V}) \tag{31}$$

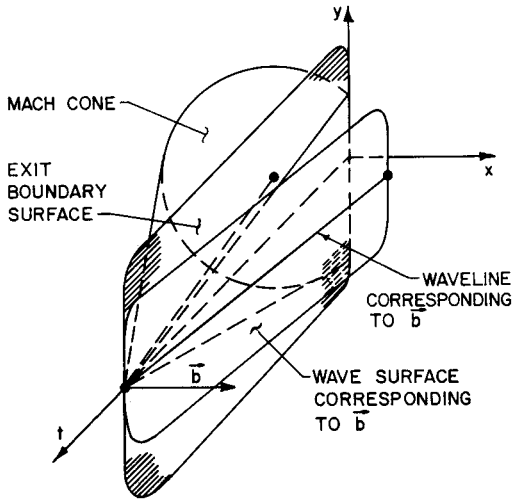


Fig. 2 Subsonic exit boundary point unit process.

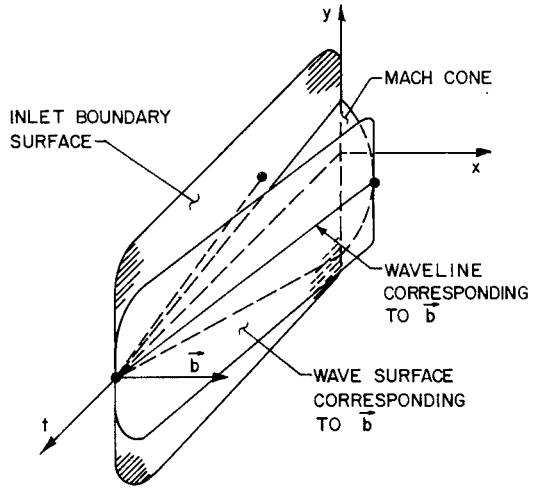


Fig. 3 Subsonic inlet boundary point unit process.

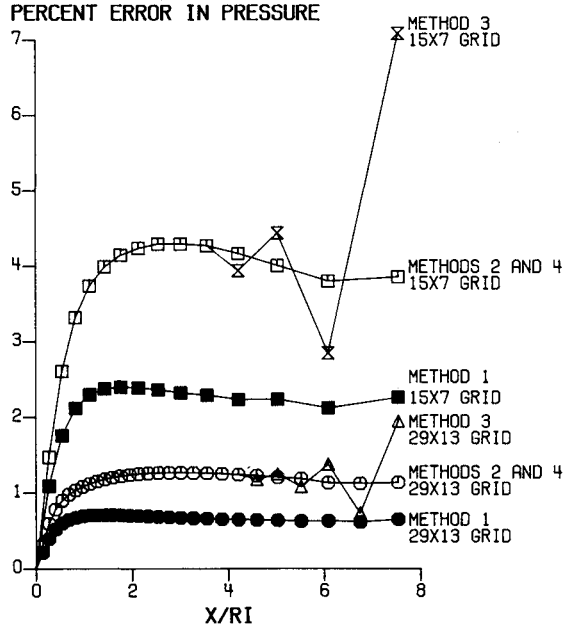


Fig. 4 Supersonic source flow wall pressure error distributions.

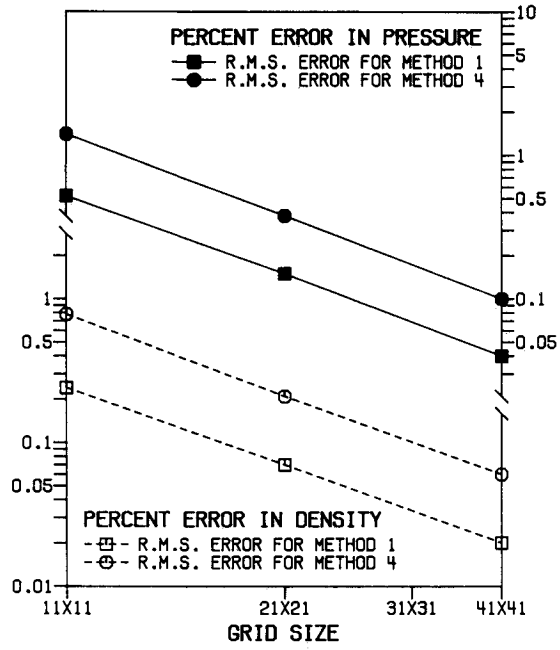


Fig. 5 Supersonic source flow errors.

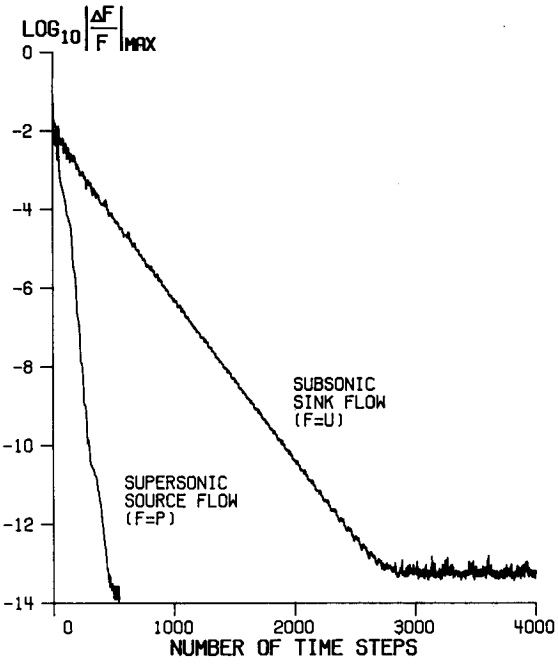


Fig. 6 Supersonic source flow and subsonic sink flow convergence histories.

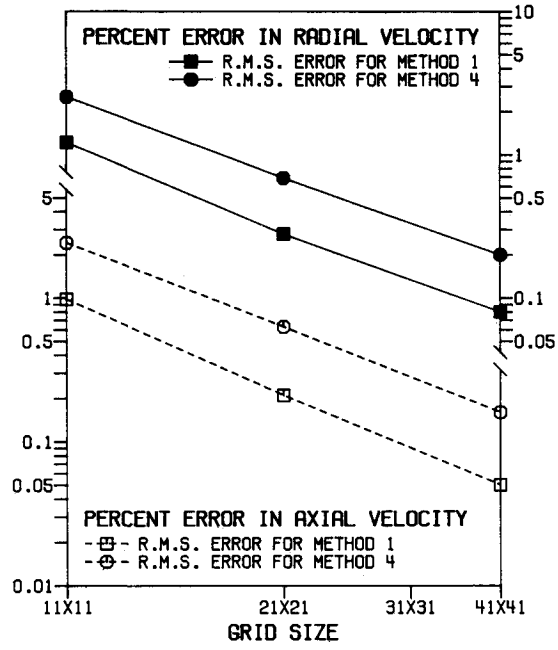


Fig. 7 Subsonic sink flow errors.

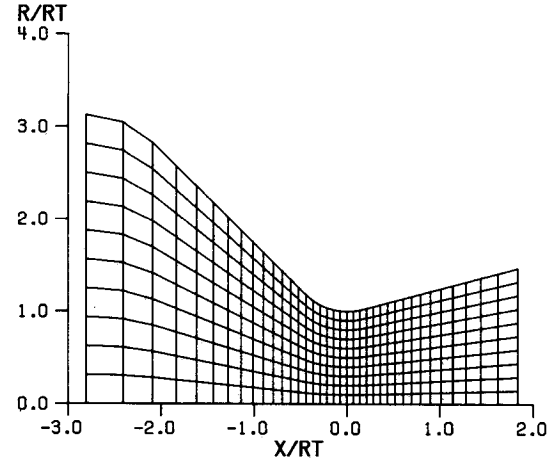


Fig. 8 Subsonic/transonic conical nozzle geometry and computational grid.

where $\bar{b}$ is the inward-pointing unit vector normal to the inlet boundary and $\bar{\delta}$ is a vector determined from the unit vector $\bar{b}$ and the two flow angles that specify the flow direction at the inlet boundary.

The governing equations, Eqs. (1-3), are replaced with the equivalent characteristic compatibility equations, Eqs. (13) and (14), at a subsonic inlet boundary point. The waveline equation, Eq. (14), is applied in the four wave hypersurfaces corresponding to the wave hypersurface unit normal vectors $\bar{n}_i$ $(i=1,2,3,4)$ given by Eq. (12). The wave hypersurface unit normal vectors $\bar{n}_i$ $(i=1,2,3)$ are chosen such that they are in directions pointing outside the computational flowfield. The wave hypersurface unit normal vector $\bar{n}_4$ is chosen such that it is equal to the inward-pointing unit vector $\bar{b}$ normal to the inlet boundary. Th pathline and the wave hypersurfaces corresponding to the wave hypersurface unit normal vectors $\bar{n}_i$ $(i=1,2,3)$ are outside the computational flowfield. Thus, the pathline equation and the waveline equations corresponding to those wave hypersurfaces are discarded and replaced with the boundary conditions, Eqs. (29-31). This situation is illustrated for unsteady two-dimensional flow in Fig. 3.

The applicable equations at a subsonic inlet boundary point are the waveline equation, Eq. (14), applied in the wave hypersurface corresponding to the wave hypersurface unit normal vector $\bar{n}_4$ and the boundary conditions, Eqs. (29-31). For a subsonic inlet boundary point unit process based on the method of characteristics, Eqs. (29-31) and the waveline equation are solved in an iteratve manner.

If the stagnation temperature and pressure are constant in time, then an expression relating the partial derivatives with respect to the time of the velocity vector and the static pressure can be obtained which eliminates the need for an iterative procedure. This expression, which is equivalent to the stagnation pressure boundary condition, Eq. (30), is

$$P_t + \rho \bar{V} \cdot \bar{V}_t = 0 \tag{32}$$

The use of Eq. (32) eliminates the need for an iterative scheme to obtain the velocity vector solution. An expression

for the partial derivative with respect to time of the velocity vector can be obtained by combining Eqs. (31) and (32) and the waveline equation, Eq. (14). This expression is given by

$$\bar{V}_t = \bar{\delta}\frac{\rho a\bar{b}\cdot\bar{M} - E - a^2 C}{\rho(a\bar{b}\cdot\bar{\delta} + \bar{\delta}\cdot\bar{V})} \tag{33}$$

The static pressure and the density can be obtained by rewriting the stagnation temperature and pressure functional relationships, Eqs. (29) and (30), as

$$P = P(T_0, P_0, V) \tag{34}$$

$$\rho = \rho(T_0, P_0, V) \tag{35}$$

At a supersonic inlet boundary point, the velocity normal to the inlet boundary is greater than or equal to the speed of sound. The pathline and all wave hypersurfaces are always outside of the computational flowfield. Thus, the pathline equation and the four waveline equations are discarded and replaced with the specification of all flow properties.

## Method of Solution

The MacCormack explicit method[10] is employed to determine the flowfield solution. The predictor and corrector steps are applied to the interior point and boundary point equations to advance the solution in time.

The backward and forward space differencing in the MacCormack method requires flow properties outside of the computational flowfield to obtain the flow property partial derivatives normal to the boundaries. Consequently, the MacCormack method must be modified at the boundaries. The following two procedures were evaluated for all types of boundary points:

1) First-order one-sided differencing normal to the boundaries in both the predictor and corrector steps.

2) Second-order extrapolation for the flow properties at the points outside of the boundaries, followed by the standard MacCormack method.

Based on supersonic source flow and subsonic sink flow error comparisons, the second procedure was found to be the most accurate, except at a subsonic inlet boundary point. This procedure also has the advantage that the MacCormack method is used unmodifed and second-order accuracy in space and time is retained. At a subsonic inlet boundary point, the two procedures were found to have similar accuracy, and the first procedure was found to be the most robust for determining the flow property partial derivatives normal to the inlet boundary. Consequently, the second procedure is used at solid and exit boundary points, and the first procedure is used at inlet boundary points.

## Overall Numerical Algorithm

The solution surface at each time level is obtained by applying the various unit processes (for a particular thermodynamic model), a specified geometry, a given set of boundary conditions, and a specified initial-value surface.

The thermodynamic model is that of a thermally and calorically perfect gas. The initial values for all of the flow properties must be specified at every computational grid location. The initial values for the density, the velocity magnitude, and the static pressure are obtained from a steady, quasi-one-dimensional, variable-area, isentropic flow analysis. The velocity components are obtained by linearly varying the flow angle such that the velocity vector at a solid boundary point is tangent to the solid boundary.

A cylindrical coordinate system is used to define the physical space. A body-fitted computational grid is generated by simple analytic functions. The axial grid locations are determined by an arctangent function. The radial and angular grid locations are determined by linear functions.

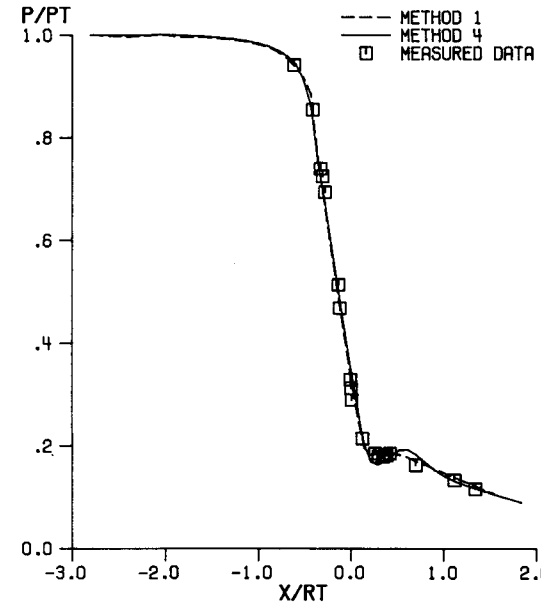


**Fig. 9 Subsonic/transonic conical nozzle wall pressure distributions.**

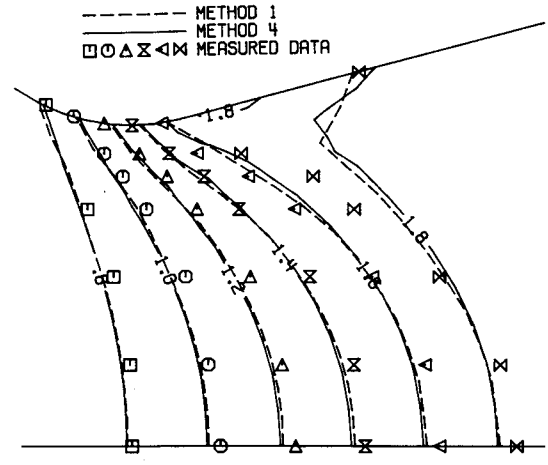


**Fig. 10 Subsonic/transonic conical nozzle Mach number contours.**

A direct marching method is employed to obtain the transient solution. The time step between successive solution surfaces is determined from the Courant-Friedrichs-Lewy (CFL) stability criterion.[11] Steady flow solutions are obtained as the asymptotic solution in time. The local time step based on the CFL stability criterion is employed in steady flow calculations to accelerate the steady-state convergence. Steady-state convergence is assumed when the maximum relative change in the axial velocity component and the static pressure between successive solution surfaces is less than a specified tolerance.

## Results

Several flowfields were analyzed to compare the computed results of the present method with exact solutions, measured data, and computed results using existing methods. The methods considered are presented in Table 1. Each of the methods listed in Table 1 was developed for calculating unsteady three-dimensional inviscid flowfields.

Method 1 employs the bicharacteristic method developed by Marcum and Hoffman[12] at all flowfield points. That method is based on Butler's method[13] and involves the numerical construction of a bicharacteristic network along which the characteristic compatibility equations are solved. At boundary points the applicable characteristic compatibil-

**Table 1 Methods considered**

| Method | Interior point algorithm | Boundary point algorithm |
|---|---|---|
| 1 | Method of characteristics | Method of characteristics |
| 2 | MacCormack method | Method of characteristics |
| 3 | MacCormack method | Present method using procedure 1 |
| 4 | MacCormack method | Present method using procedure 2 |

ity relations are solved simultaneously with the boundary conditions. Method 2 employs the MacCormack explicit method[10] at all interior points and the bicharacteristic method of Marcum and Hoffman[12] at all boundary points. Methods 3 and 4 employ the MacCormack explicit method at all interior points and the procedures developed in the present investigation at all boundary points. Method 3 uses the first-order-accurate differencing procedure to evaluate derivatives normal to the boundaries (i.e., procedure 1). Method 4 uses the second-order-accurate differencing procedure (i.e., procedure 2) to evaluate the derivatives normal to the boundaries.

### Supersonic Source Flow Study

A steady spherical supersonic source flow was analyzed to verify the computed results against a known exact solution. The flowfield considered lies between the vertical lines defined by the location where the specified initial Mach number $M_i$ occurs on the axis and the specified exit Mach number $M_e$ occurs on the conical wall. The specific heat ratio is 1.4, the inlet Mach number $M_i$ is 1.5, the exit Mach number $M_e$ is 4.0, and the source flow angle $\theta_s$ is 15 deg.

The percent error in the wall static pressure as a function of normalized axial position (normalized with the inlet radius) for methods 1 to 4 for a $15\times7$ and a $29\times13$ grid is presented in Fig. 4. Methods 2 and 4 have identical errors within the resolution of Fig. 4. The errors for methods 2 and 4 are roughly double the errors for method 1. However, the errors are quite reasonable, and both of these methods are good procedures. The second-order accuracy of all of the methods is verified by comparing the errors for the two different grid sizes presented in Fig. 4. Method 3 misbehaves at the exit due to the first-order space differencing normal to the boundary. The oscillatory error behavior for this method is unacceptable. This behavior is eliminated by using a second-order extrapolation for the flow properties outside the boundary followed by the standard MacCormack method, method 4.

The root mean square error in the static pressure and density as a function of grid size for methods 1 and 4 are presented in Fig. 5. For these results, the specific heat ratio is 1.4, the inlet Mach number $M_i$ is 1.5, the exit Mach number $M_e$ is 3.0, and the source flow angle $\theta_s$ is 30 deg. The static pressure and the density were found to be the least accurately computed flow properties in a supersonic source flow. These results show that method 1 is the most accurate and that the present method, method 4, yields acceptable results. The second-order accuracy of methods 1 and 4 is clearly evident in Fig. 5.

The maximum relative change in the static pressure between successive solution surfaces as a function of the number of time steps for the present method (method 4) for a supersonic source flow with a $21\times21$ grid is presented in Fig. 6. For the Cyber 205 using 64-bit word arithmetic, steady-state convergence to 0.001% required 200 time steps and convergence to machine accuracy required 500 time steps.

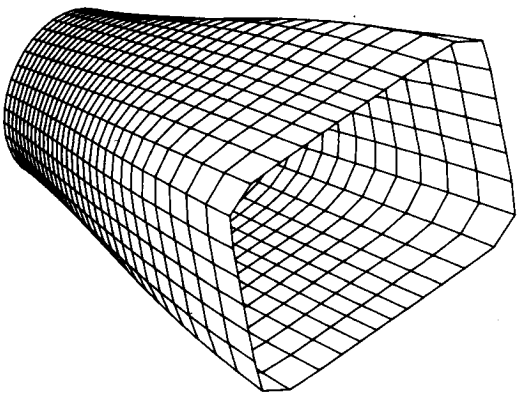

**Fig. 11 Supersonic super-elliptical nozzle geometry and computational grid.**

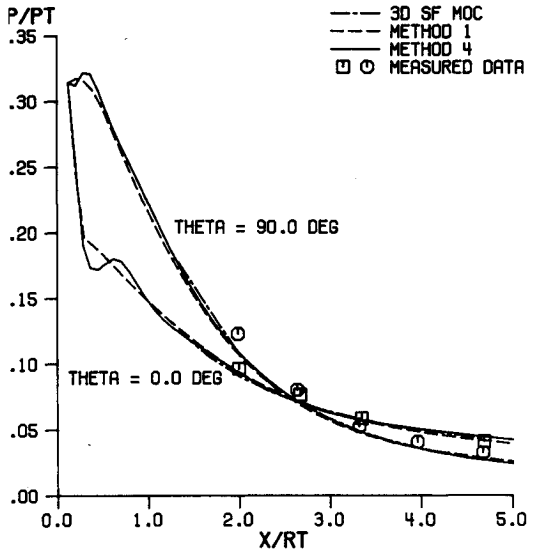


**Fig. 12 Supersonic super-elliptical nozzle wall pressure distributions.**

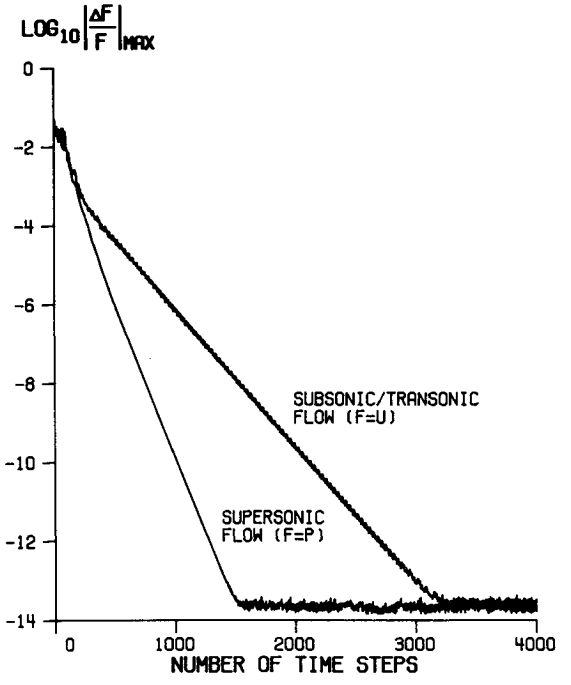


**Fig. 13 Supersonic super-elliptical nozzle convergence histories.**

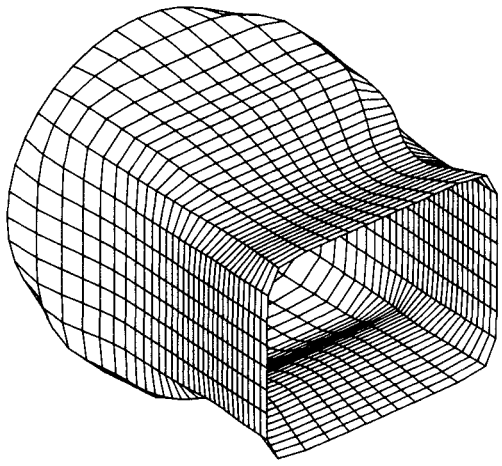

**Fig. 14 Subsonic/transonic super-elliptical nozzle geometry and computational grid.**

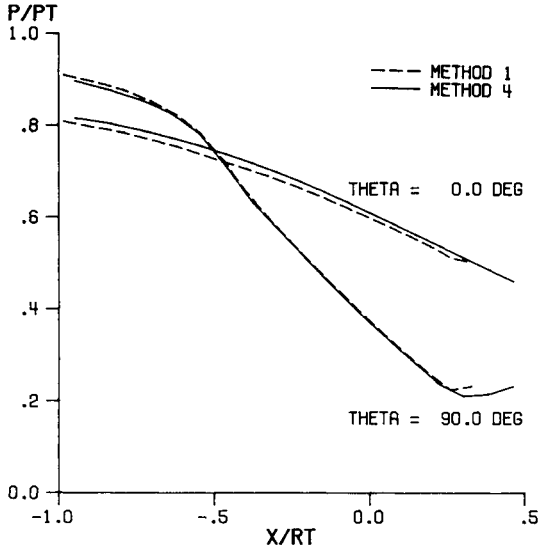


**Fig. 15 Subsonic/transonic super-elliptical nozzle wall pressure distributions.**

### Subsonic Sink Flow Study

A steady spherical subsonic sink flow was analyzed to verify the computed results against a known exact solution. The flowfield considered lies between the vertical lines defined by the location where the specified initial Mach number $M_i$ occurs on the conical wall and the specified exit Mach number $M_e$ occurs on the axis. The specific heat ratio is 1.4, the inlet Mach number $M_i$ is 0.1, the exit Mach number $M_e$ is 0.6, and the sink flow angle $\theta_s$ is 30 deg.

The root mean square error in the axial and radial velocity components as a function of grid size for methods 1 and 4 are presented in Fig. 7. The axial and radial velocity components were found to be the least accurately computed flow properties in a subsonic sink flow. These results show that method 1 is the most accurate and that the present method, method 4, yields acceptable results. The second-order accuracy of methods 1 and 4 is clearly evident in Fig. 7.

The maximum relative change in the axial velocity component between successive solution surfaces as a function of the number of time steps for the present method (method 4) for a subsonic sink flow with a $21 \times 21$ grid is presented in Fig. 6. For the Cyber 205 using 64-bit word arithmetic, steady-state convergence to 0.001% required 700 time steps and convergence to machine accuracy required 2700 time steps.

### Subsonic/Transonic Conical Nozzle Study

The steady axisymmetric subsonic/transonic flowfield in the conical nozzle investigated experimentally by Cuffel, Back, and Massier[14] was analyzed to verify the computed results against measured data. The geometry of the conical nozzle and the $38 \times 11$ computational grid are illustrated in Fig. 8. The specific heat ratio is 1.4.

The normalized wall static pressure (normalized with the nozzle inlet stagnation pressure) as a function of normalized axial position (normalized with the nozzle throat radius) for methods 1 and 4 and the measured data of Cuffel et al. is presented in Fig. 9. Mach number contours in the transonic region for methods 1 and 4 and the measured data of Cuffel et al. are presented in Fig. 10. The results of the present method, method 4, are in good agreement with the results of method 1 and the measured data of Cuffel et al. Steady-state convergence of 0.001% required 1500 time steps.

### Supersonic Super-Elliptical Nozzle Study

The steady three-dimensional supersonic flowfield in the super-elliptical nozzle which was investigated experimentally and analytically by Ransom, Hoffman, and Thompson,[15] was analyzed to verify the computed results against measured data. The geometry of this nozzle and the $31 \times 11 \times 10$ computational grid are illustrated in Fig. 11. The specific heat ratio is 1.4. The initial-value plane used by Ransom et al. was used as the inlet plane initial data for methods 1 and 4.

The normalized wall static pressure (normalized with the nozzle inlet stagnation pressure) in the two planes of symmetry as a function of normalized axial position (normalized with the nozzle throat radius) for methods 1 and 4, the steady flow method of characteristics algorithm developed by Ransom et al. (3D SF MOC), and the measured data of Ransom et al. is presented in Fig. 12. The results of the present method, method 4, are in very good agreement with the results of method 1, the results of Ransom et al., and the measured data of Ransom et al. The location where the pressure distributions in the two planes of symmetry intersect is predicted very well by all three methods.

The maximum relative change in the static pressure between successive solution surfaces as a function of the number of time steps for the present method (method 4) for the supersonic super-elliptical nozzle is presented in Fig. 13. For the Cyber 205 using 64-bit word arithmetic, steady-state convergence to 0.001% required 400 time steps and convergence to machine accuracy required 1500 time steps.

### Subsonic/Transonic Super-Elliptical Nozzle Study

The steady three-dimensional subsonic/transonic flowfield in a super-elliptical nozzle was analyzed to compare the results of the present method and the results of method 1. The geometry of this nozzle and the $31 \times 11 \times 10$ computational grid are illustrated in Fig. 14. The specific heat ratio is 1.3.

The normalized wall static pressure (normalized with the nozzle inlet stagnation pressure) in the two planes of symmetry as a function of normalized axial position (normalized with the nozzle throat radius in the plane of symmetry at $\theta = \pi/2$) for methods 1 and 4 is presented in Fig. 15. The results of the present method, method 4, are in good agreement with the results of method 1.

The maximum relative change in the axial velocity component between successive solution surfaces as a function of the number of time steps for the present method (method 4) for the subsonic/transonic super-elliptical nozzle is presented in Fig. 13. For the Cyber 205 using 64-bit word arithmetic, steady-state convergence to 0.001% required 700 time steps and convergence to machine accuracy required 3200 time steps.

**Table 2 Computational time**

| Computer | Code | CPU time[a] | Rate of computation[b] |
|---|---|---|---|
| Cyber 205 | Scalar(SP)[c,e] | 159 | 66.4 |
| With FTN 200 | Scalar[d,e] | 62 | 25.8 |
| Version 2.2 | Vector[d,e,g] | 11 | 4.7 |
| Compiler | Vector(32)[d,f,g] | 7 | 3.1 |
| Cray X-MP | Scalar[e] | 57 | 23.7 |
| With CFT | Vector[e,h] | 13 | 5.3 |
| Version 1.14 | — | — | — |
| Compiler | — | — | — |

[a]CPU time in seconds required to compute 700 time steps with a $31 \times 11 \times 10$ grid. [b]Microseconds of CPU time required per time step per grid point. [c]All arrays assigned to dynamic space and mapped into small pages (2048 words/page). [d]All arrays and descriptors assigned to dynamic space and mapped into large pages (65,536 words/page). [e]64-bit word arithmetic. [f]32-bit word arithmetic. [g]Vectorized using explicit vector instructions. [h]Vectorized using a combination of compiler-generated vector instructions and explicit vector instructions.

### Computational Time

The CPU time and rate of computation for the present method, method 4, for scalar and vector codes executed on the Cyber 205 and Cray X-MP computers are presented in Table 2. All of the CPU intensive code contained within the time step loop was vectorized for the vector codes listed in Table 2. The present method is approximately eight times faster than the full method of characteristics algorithm, method 1, and is approximately four times faster than the combined MacCormack method and method of characteristics algorithm, method 2. The rate of convergence for the present method is also greater than that for either method 1 or 2.

Variations of the Cyber 205 code are listed in Table 2 to illustrate the effects of page size and precision on the CPU time. The Cyber 205 allows arrays and dynamic space to be mapped into small or large pages. A considerable increase in the CPU time occurs if the arrays are mapped into small pages and the individual array sizes are larger than a small page. Mapping common blocks into large pages or assigning arrays to dynamic space and mapping dynamic space into large pages eliminates this problem.

The Cyber 205 also allows the use of either 32- or 64-bit word arithmetic. The 32-bit vector code listed in Table 2 is approximately 1.5 times faster than the 64-bit vector code for a $31 \times 11 \times 10$ grid. A maximum speed-up factor of roughly 1.9 is obtainable with the present method for grids with 30,000 or more grid points.

## Conservative Variables

The governing equations expressed in primitive variables are employed in the present investigation. For flowfields with strong shock waves, explicit shock wave fitting may be required with the present method. In such cases it would be advantageous to use a conservative variable version of the present method. The method of characteristics procedure used in the present investigation to develop the equations applicable at boundary points is based on primitive variables. However, the resulting equations can be transformed into conservative variables. These equations have been implemented in a conservative variable version of the program based on method 4 in Table 1. Preliminary results for supersonic source flow and subsonic sink flow indicate that the conservative variable and primitive variable versions yield very similar results.

## Conclusions

A numerical boundary condition procedure based on a variation of the method of characteristics due to Kentzer has been developed for solving inviscid flowfields by finite-difference methods. This procedure was used to develop a second-order-accurate numerical algorithm using the MacCormack explicit method. For steady flowfields, the accuracy of the present method was found to be comparable to that of a full bicharacteristic method and nearly identical to that of a combined MacCormack and bicharacteristic method. Solutions obtained with the present method agree well with solutions obtained with method of characteristics algorithms and experimental data for two-dimensional and three-dimensional nozzle flowfields. Although the procedure was verified only for steady flowfields, it is equally applicable to unsteady flowfields.

## References

[1]"Numerical Boundary Condition Procedures," NASA Conference Pub. 2201, Oct. 1981.

[2]Abbett, M.J., "Boundary Condition Calculation Procedures for Inviscid Supersonic Flow Fields," *Proceedings of the AIAA Computational Fluid Dynamics Conference*, Palm Springs, CA, July 1973, pp. 153–172.

[3]Kentzer, C.P., "Discretization of Boundary Conditions on Moving Discontinuities," *Lecture Notes in Physics*, Vol. 8, Springer-Verlag, New York, pp. 108–113.

[4]Brown, J.J. and Hoffman, J.D., "Unsteady Three-Dimensional Flow in Rotating Rocket Motor Nozzles," *Journal of Spacecraft and Rockets*, Vol. 23, March–April 1986, pp. 207–214.

[5]Chakravarthy, S.R., "Euler Equations—Implicit Schemes and Boundary Conditions," *AIAA Journal*, Vol. 21, May 1983, pp. 699–706.

[6]Rusanov, V.V., "The Characteristics of General Equations of Gas Dynamics," *Zhurnal Vychislitelnoi Mathematiki Mathematicheskoi Fiziki*, Vol. 3, 1963, pp. 508–527.

[7]Hoffman, J.D., "The Method of Characteristics Applied to Unsteady One-, Two-, and Three-Dimensional Flows," School of Mechanical Engineering, Purdue University, West Lafayette, IN, Rept. TR-80-07, June 1980.

[8]Zucrow, M.J. and Hoffman, J.D., *Gas Dynamics*, Vols. 1 and 2, John Wiley, New York, 1975.

[9]Marcum, D.L., "Calculation of Three-Dimensional Inviscid Flowfields in Propulsive Nozzles with Centerbodies," Ph.D. Thesis, Purdue Univ., West Lafayette, IN, Aug. 1985.

[10]MacCormack, R.W., "The Effect of Viscosity in Hypervelocity Impact Cratering," AIAA Paper 69-354, April 1969.

[11]Courant, R., Friedrichs, K.O., and Lewy, H., "Uber die Partiellen Differenzialgleichungen der Mathematischen Physik," *Mathematische Annalen*, Vol. 100, 1928, pp. 32–74.

[12]Marcum, D.L. and Hoffman, J.D., "Calculation of Three-Dimensional Subsonic/Transonic Inviscid Flowfields by the Unsteady Method of Characteristics," *AIAA Journal*, Vol. 3, Oct. 1985, pp. 1497–1505.

[13]Butler, D.S., "The Numerical Solution of Hyperbolic Systems of Partial Differential Equations in Three Indpendent Variables," *Proceedings of the Royal Society of London*, Vol. 255A, 1960, pp. 232–252.

[14]Cuffel, R.F., Back, L.H., and Massier, P.F., "Transonic Flowfield in a Supersonic Nozzle with Small Throat Radius of Curvature," *AIAA Journal*, Vol. 7, July 1969, pp. 1364–1366.

[15]Ransom, V.H., Hoffman, J.D., and Thompson, H.D., "A Second-Order Bicharacteristics Method for Three-Dimensional, Steady, Supersonic Flow," *AIAA Journal*, Vol. 10, Dec. 1972, pp. 1573–1581.